

Jet Cross Sections at HERA - Current Issues

Steve Maxfield (Dept. of Physics, University of Liverpool),
Björn Pötter (Max-Planck-Institut für Physik, München, Germany)
and Laurel Sinclair (Department of Physics and Astronomy, Glasgow University)

*to appear in the proceedings of the 3rd UK Phenomenology Workshop
on HERA Physics, September 1998, Durham.*

Abstract

Since the start of HERA operation there has been considerable progress in the understanding of jet production in ep collisions. QCD calculations are now able to accommodate the hadronic structure of the virtual photon. The luminosities delivered by HERA are now sufficient to allow studies of final states in which more than two high transverse energy jets are produced. The transition between jet processes in photoproduction and in deep inelastic scattering has been studied in some detail. These advances are highlighted here.

1 Dijet Cross Sections at Low Q^2 and Virtual Photon Structure

1.1 Comparing Dijet Cross Sections with NLO QCD Calculations

H1 have measured the triple-differential cross-section, $d^3\sigma_{ep}/dQ^2 d\overline{E}_T^2 dx_\gamma^{jets}$ (\overline{E}_T^2 is the mean E_T of the two highest E_T jets) in the γ^*p center-of-mass system (hadronic cms) [1]. The photon virtuality spans the range $1.6 < Q^2 < 80 \text{ GeV}^2$ and $y = Pq/Pk$ is constrained to $0.1 < y < 0.7$, where P , q and k are the four-vectors of the proton, virtual photon, and electron. The momentum fraction of the parton from the photon entering the hard scattering, x_γ^{jets} , defined as

$$x_\gamma^{jets} = \frac{\sum_{i=1,2} E_{T_i}^{jets} \exp(-\eta_i^{jets})}{W} \quad (1)$$

is estimated from the two highest E_T jets. The variable $W^2 = (P + q)^2 = 2Pq - Q^2$ defines the hadronic cms energy.¹⁾ The triple differential cross-section is shown in figure 1 as a function of x_γ^{jets} in ranges of Q^2

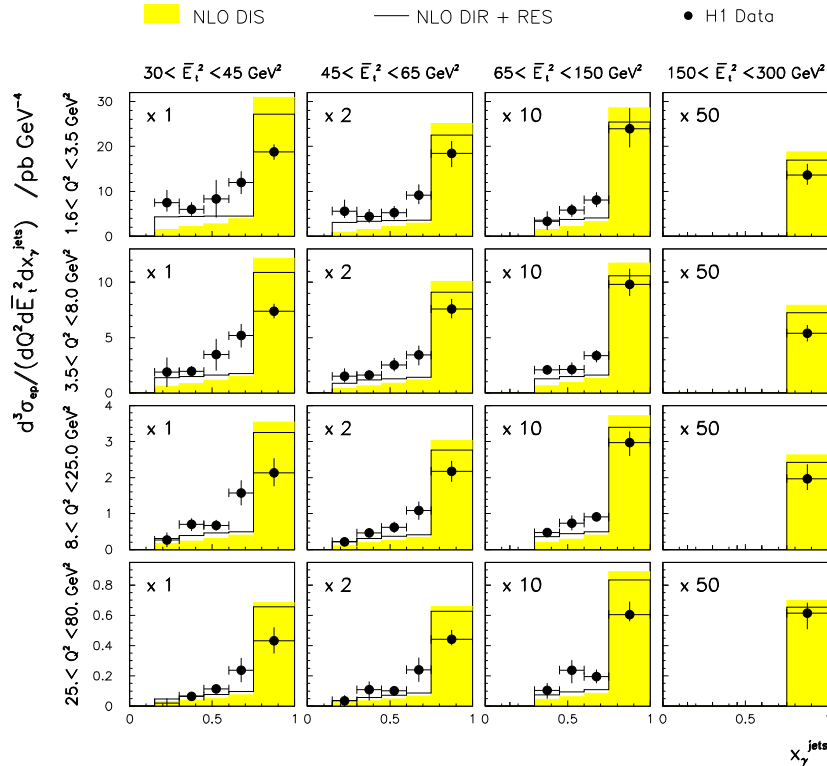


Figure 1: The differential dijet cross-section $d^3\sigma_{ep}/dQ^2 d\overline{E}_T^2 dx_\gamma^{jets}$ shown as a function of x_γ^{jets} for different regions of \overline{E}_T^2 and Q^2 compared to a NLO QCD calculation which employed the SaS1M PDF's of the virtual photon. The direct component of this model is shown as the shaded histogram. The result including a resolved component in NLO is shown as the full line.

and \overline{E}_T^2 . The data (points) are corrected for detector effects and the error bar shows the quadratic sum of systematic and statistical errors. The cross section decreases rapidly with increasing \overline{E}_T^2 and with increasing Q^2 . Hadronization corrections are not included in the data. These are believed to be small on average but will presumably change the shape of the x_γ^{jets} distribution.

QCD calculations of dijet cross-sections with virtual photons have recently been performed at next-to-leading order (NLO) [2, 3]. The calculations are implemented in the fixed order program **JetViP** [4]. In NLO, in the

¹⁾One can theoretically define the variable $x_\gamma = p_0 P / q P$, where $p_0 = x_\gamma q$ is the four-vector of the incoming parton from the photon. This definition assumes a collinear emission of the parton from the photon, which is an approximation neglecting some k_\perp contribution due to the finite Q^2 . These contributions are, however, small for moderate Q^2 . This variable differs from that defined in (1). When comparing with QCD calculations at LO level, partons directly give jets and there are exactly two partons in the final state. Thus, $x_\gamma^{jets} = x_\gamma$. However, in NLO, x_γ still gives the momentum fraction of the parton in the photon, but $x_\gamma^{jets} \neq x_\gamma$. At NLO, one also has contributions to $x_\gamma^{jets} < 1$ from the direct contribution, whereas at LO $x_\gamma^{jets} = 1$ for the direct process.

direct component a logarithm $\ln E_T^2/Q^2$ occurs, which is proportional to the photon splitting function. This term is large for $E_T^2 \gg Q^2$ and therefore subtracted and resummed in the virtual photon structure function. The condition $E_T^2 \gg Q^2$ ensures that it is possible to resolve an internal structure of the virtual photon. The virtual photon PDF's are suppressed as $Q^2 \rightarrow E_T^2$ and various anzätze have been used to interpolate between the regions of known leading-log behaviour [5, 6, 7, 8]. It should be noted that the logarithmic term is only subtracted for the transversely polarized photons, since it vanishes in the case of longitudinally polarized photons for $Q^2 \rightarrow 0$. The hadronic content of longitudinal virtual photons should be very small and therefore negligible. The results of the NLO calculations are also shown in figure 1. The direct component of this model is shown as the shaded histogram. The result including a resolved component in NLO is shown as the full line. The calculation including a resolved photon component compares better to the data and indicates a need for a resolved virtual photon component below 10 GeV², especially in the forward rapidity region, corresponding to low x_γ^{jets} . The discrepancy of data and NLO calculation for $x_\gamma^{jets} > 0.75$ will presumably be cured when hadronization effects are considered, which lower the NLO results at large x_γ^{jets} .

1.2 Effective Virtual Photon Parton Densities

H1 have used their studies to extract an effective parton density (EPDF) of the virtual photon. By using the Single Effective Subprocess Approximation [9], the cross-section for dijet production in LO can be written

$$\frac{d^5\sigma}{dy dx_\gamma dx_p d\cos\theta^* dQ^2} \sim \frac{f_{eff/\gamma}^k(x_\gamma, P_t^2, Q^2)}{x_\gamma} \frac{f_{eff/p}(x_p, P_t^2)}{x_p} |M_{SES}(\cos\theta^*)|^2.$$

Here the Effective Parton Densities (EPDF), $f_{eff/\gamma}^k$ and $f_{eff/p}$, are defined as $f_{eff/A} \equiv (f_{q/A} + f_{\bar{q}/A}) + \frac{9}{4}f_{g/A}$. The EPDF is shown in figure 2. We see that, independently of Q^2 , the parton density tends to be flat or rising

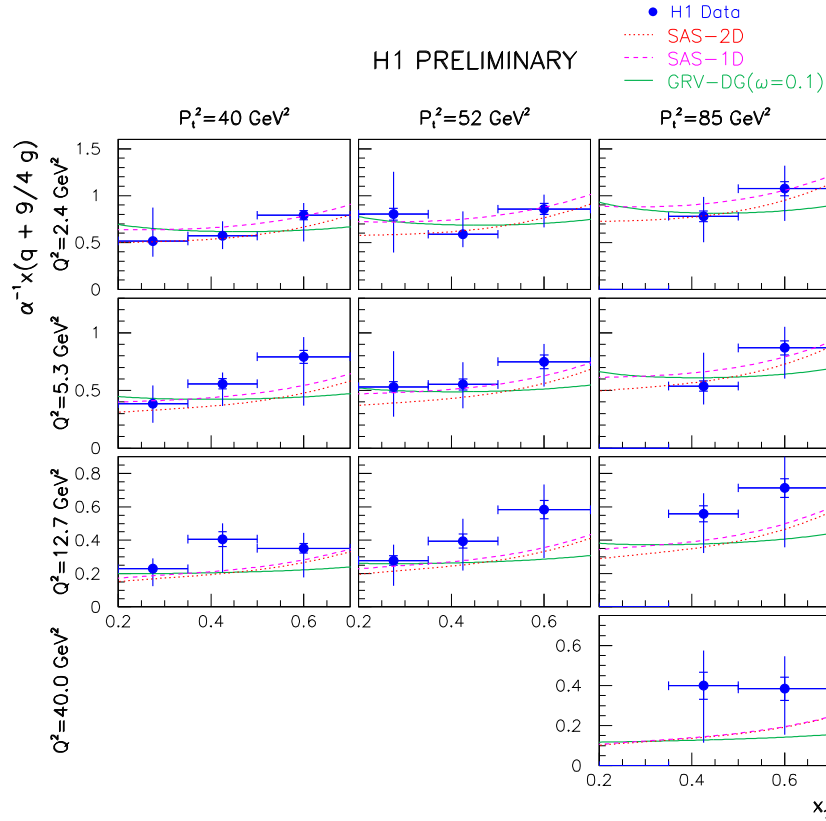


Figure 2: The leading order effective parton density of the photon $x(q + 9/4g)$, divided by the fine structure constant α , as a function of x_γ for different values of Q^2 and the transverse momentum P_t^2 . The data are displayed as points, with the inner error bar depicting the statistical error, and the total error bar the quadratic sum of statistical and systematic errors. Also shown are the prediction from the DG model using GRV-LO real photon parton densities and $\omega = 0.1$ (solid line) and the SAS-1D (dashed line) and SAS-2D(dot-dashed line) parameterisations.

with x_γ (not to be confused with x_γ^{jets}). This behaviour is maintained as the probing scale increases. These are features characteristic of photon structure. The data are compared with predictions from the SaS [5] and DG [7, 8] models which are able to describe the data quite well except where $Q^2 \rightarrow P_t^2$ and various aspects of the model start to break down. The models tend to underestimate the data in these regions. The three parameterisations for the parton density all give a good description of the data both in the lowest x_γ range and in the lowest two Q^2 bins but predict a more rapid suppression as $Q^2 \rightarrow P_t^2$ than is seen in the data.

2 Three Jet Photoproduction

ZEUS has measured the high-mass three-jet cross section in photoproduction, $d\sigma/dM_{3J}$, as shown in Figure 3 [10]. The $\mathcal{O}(\alpha_s^2)$ pQCD calculations from two groups of authors [11, 12] provide a good description of

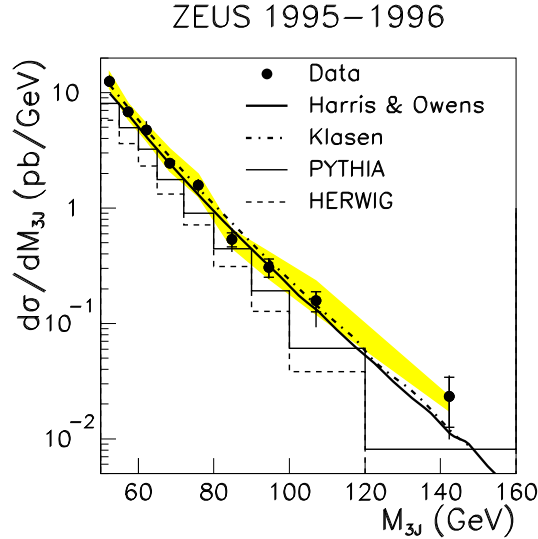


Figure 3: The three-jet cross section $d\sigma/dM_{3J}$. The dots show the data. The inner error bars show the statistical error. The outer error bars show the quadratic sum of the statistical and systematic uncertainties with the exception of the absolute energy scale uncertainty which is shown separately as a shaded band. $\mathcal{O}(\alpha_s^2)$ pQCD calculations by two groups of authors are shown by thick solid and dot-dashed lines. The thin solid and dashed histograms show the predictions from PYTHIA and HERWIG.

the data, even though they are leading order for this process. Monte Carlo models also generate three-jet events through the parton shower mechanism and both PYTHIA [13] and HERWIG [14] reproduce the shape of the M_{3J} distribution.

For three-jet events there are two relevant scattering angles as illustrated in Figure 4(a). The distributions of $\cos\theta_3$ and ψ_3 are shown in Figure 4(b) and (c). The $\cos\theta_3$ distribution resembles that of $\cos\theta^*$ in dijet production [15] and exhibits forward and backward peaks. It is well described in both $\mathcal{O}(\alpha_s^2)$ pQCD calculations and parton shower models. The ψ_3 distribution is peaked near 0 and π indicating that the three-jet plane tends to lie near the plane containing the highest energy jet and the beam. This is particularly evident if one considers the ψ_3 distribution for three partons uniformly distributed in the available phase space. The phase space near $\psi_3 = 0$ and π has been depleted by the E_T^{jet} cuts and by the jet-finding algorithm. The pQCD calculations describe perfectly the ψ_3 distribution. It is remarkable that the parton shower models PYTHIA and HERWIG are also able to reproduce the ψ_3 distribution.

Within the parton-shower model it is possible to determine the contribution to three-jet production from initial-state radiation (ISR) and final-state radiation. It is also possible to switch the QCD phenomenon of colour coherence on and off. From a Monte Carlo study it has been determined that ISR is predominantly responsible for three-jet production. Also, it has been found that colour coherence can account for the suppression of large angle emissions which leads to the depletion of the ψ_3 distribution near $\psi_3 = \pi/2$ [10].

3 Summary

The dijet cross section at low Q^2 has been measured by the H1 collaboration and compared to NLO QCD calculations. The comparison shows a clear need for resolved virtual photon component. First measurements

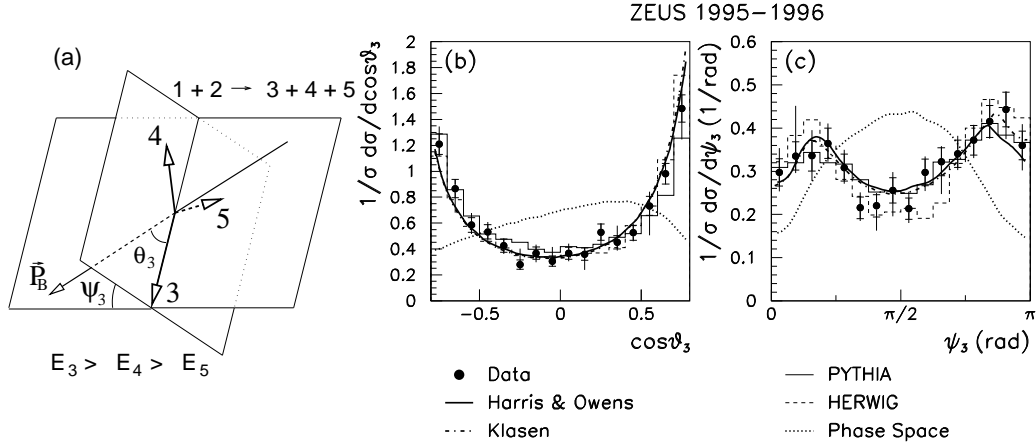


Figure 4: (a) Centre-of-mass frame diagram of the three-body scattering angles. The beam direction is indicated by \vec{P}_B . Distributions of $\cos\theta_3$ and ψ_3 are shown in (b) and (c). The dotted curve shows the distribution for a constant matrix element. Other details are as described for Figure 3.

of a leading order effective virtual photon PDF have been made. Existing models for virtual photon PDF's are consistent with the measurements but systematic errors are still large.

A first measurement of high transverse energy three-jet photoproduction has been performed. The distribution of the three jets is sensitive to colour coherence and is correctly predicted in $\mathcal{O}(\alpha\alpha_s^2)$ pQCD.

References

- [1] H1 Collaboration, C. Adloff et al., DESY-98-205 [hep-ex/9812024], to be published in Eur. Phys. J. C.
- [2] M. Klasen, G. Kramer, B. Pötter, Eur. Phys. J. C1 (1998) 261.
- [3] G. Kramer, B. Pötter, Eur. Phys. J. C5 (1998) 665; Proceedings of the Workshop on Photon Interactions and the Photon Structure, Lund, Sweden, 10-13 Sep 1998 [hep-ph/9810450].
- [4] B. Pötter, DESY-98-071 [hep-ph/9806437] (see also <http://www.desy.de/~poetter/jetvip.html>).
- [5] T. Sjöstrand and G. A. Schuler, Phys. Lett. **B376** (1996) 193.
- [6] M. Glück, E. Reya and M. Stratmann, Phys. Rev. **D54** (1996) 5515.
- [7] M. Drees and R. Godbole, Phys. Rev. **D50** (1994) 3124.
- [8] F. Borzumati and G. Schuler, Z. Phys. **C58** (1993) 139.
- [9] B. V. Combridge, C. J. Maxwell, Nucl. Phys. **B239** (1984) 429.
- [10] ZEUS Collab., J. Breitweg et al., Phys. Lett. **B443** (1998) 394.
- [11] B.W. Harris and J.F. Owens, Phys. Rev. **D56** (1997) 4007.
- [12] M. Klasen, Eur. Phys. J. C7 (1999) 225.
- [13] H.-U. Bengtsson and T. Sjöstrand, Comp. Phys. Comm. **46** (1987) 43.
- [14] G. Marchesini et al., Comp. Phys. Comm. **67** (1992) 465.
- [15] ZEUS Collab., M. Derrick et al., Phys. Lett. **B384** (1996) 401.